

Crystal structure of Omp32, the anion-selective porin from *Comamonas acidovorans*, in complex with a periplasmic peptide at 2.1 Å resolution

K Zeth¹, K Diederichs², W Welte² and H Engelhardt^{1*}

Background: Porins provide diffusion channels for salts and small organic molecules in the outer membrane of bacteria. In OmpF from *Escherichia coli* and related porins, an electrostatic field across the channel and a potential, originating from a surplus of negative charges, create moderate cation selectivity. Here, we investigate the strongly anion-selective porin Omp32 from *Comamonas acidovorans*, which is closely homologous to the porins of pathogenic *Bordetella* and *Neisseria* species.

Results: The crystal structure of Omp32 was determined to a resolution of 2.1 Å using single isomorphous replacement with anomalous scattering (SIRAS). The porin consists of a 16-stranded β barrel with eight external loops and seven periplasmic turns. Loops 3 and 8, together with a protrusion located within β-strand 2, narrow the cross-section of the pore considerably. Arginine residues create a charge filter in the constriction zone and a positive surface potential at the external and periplasmic faces. One sulfate ion was bound to Arg38 in the channel constriction zone. A peptide of 5.8 kDa appeared bound to Omp32 in a 1:1 stoichiometry on the periplasmic side close to the symmetry axis of the trimer. Eight amino acids of this peptide could be identified, revealing specific interactions with β-strand 1 of the porin.

Conclusions: The Omp32 structure explains the strong anion selectivity of this porin. Selectivity is conferred by a positive potential, which is not attenuated by negative charges inside the channel, and by an extremely narrow constriction zone. Moreover, Omp32 represents the anchor molecule for a peptide which is homologous to proteins that link the outer membrane to the cell wall peptidoglycan.

Introduction

Porins are pore proteins that form outer membrane channels in Gram-negative bacteria, mitochondria and chloroplasts (for reviews see [1–4]). They mediate the exchange of small molecules between the outer and inner environment of bacterial cells or the organelles. Bacterial porins usually occur as trimers and have been classified into specific and unspecific pore proteins. Unspecific porins are water-filled channels facilitating the passive diffusion of ions, nutrients and metabolites up to a molecular mass of ~600 Da [2]. These porins do not appear to be specific for certain molecules but might effectively select anions or cations. Specific porins contain substrate-binding sites that lead to an efficient uptake of compounds such as sucrose, maltose or cyclodextrins [5–7].

As a characteristic for bacterial outer membrane proteins in general [5,6,8–12], porins are built of amphipathic β strands that form an antiparallel β barrel. Unspecific porins possess a 16-stranded β barrel with eight connecting loops (L1–L8) of variable length and seven (eight in

Addresses: ¹Max-Planck-Institut für Biochemie, Abteilung Molekulare Strukturbiologie, Am Klopferspitz 18a, D-82152 Martinsried, Germany and ²Universität Konstanz, Fakultät für Biologie, Universitätsstraße 10, D-78457 Konstanz, Germany.

*Corresponding author.
E-mail: engelhar@biochem.mpg.de

Key words: anion-selective ion channel, electrophysiology, outer membrane protein, porin Omp32, X-ray structure

Received: 12 May 2000
Revisions requested: 20 June 2000
Revisions received: 19 July 2000
Accepted: 19 July 2000

Published: 29 August 2000

Structure 2000, 8:981–992

0969-2126/00/\$ – see front matter
© 2000 Elsevier Science Ltd. All rights reserved.

the case of OmpF and PhoE from *Escherichia coli*) short periplasmic turns. The barrel is usually of concave shape and spans the entire outer membrane. The cross-section of the pore is restricted by one large loop that folds into the channel interior narrowing the pore to about or less ~1 nm in diameter. The cross-section of the constriction zone together with the amino acid residues located inside the channel is thought to predominantly determine the physiological and conductivity properties of the pore [13,14]. The internal electrostatic field provides the ion-filter properties of the channel and might contribute to the phenomenon of voltage-dependent closing [15–17], which is not yet understood in detail [18,19].

Porins do not only function as pore proteins but in some bacteria might also be involved in linking the outer membrane to the peptidoglycan in the cell wall [20]. Binding of the outer membrane to the rigid cell wall is mediated by lipoproteins in many species [21] and by OmpA and related molecules which possess a peptidoglycan-binding periplasmic domain [22]. Cyanobacterial porins and the

porin from *Thermus thermophilus* contain a particular peptidoglycan-binding motif, the SLH domain (S-layer homology domain [23]), which is an integral part of the porin polypeptide and is linked via an extended triple coiled-coil structure to the main body of the pore protein [24]. Other Gram-negative bacteria (e.g. *Rhodospirillum rubrum*) exhibit independent genes that code for porins and proteins with peptidoglycan-binding motifs that appear to interact with each other according to experimental evidence [20]. Up to now it has not been possible to demonstrate such interactions structurally.

Porin Omp32 from *Comamonas acidovorans* is strongly anion-selective and shows further unusual functional properties particularly at low ionic strength [25]. We crystallized Omp32 [26] in order to gain further understanding of the structural basis for the particular functions and to investigate the principle structural architecture, which might also be of relevance to studies on related porins. *C. acidovorans*, recently reclassified to *Delftia acidovorans* [27], is a member of the β subdivision of proteobacteria. Related microorganisms of this group (e.g. the *Bordetellaceae* and *Neisseriaceae*) are of particular interest because of their role in various infectious diseases and programmed cell death. The role of porin PorB from *Neisseria gonorrhoeae* as an inducer of apoptosis was recently described [28]. In the absence of structural information on these proteins the prediction of folding and models of surface topology must mainly rely on biochemical data. In the light of the significant sequence similarities between porins of these organisms and Omp32, however, a more detailed model can be established on the basis of the atomic structure of the *C. acidovorans* porin.

In this paper we present the 2.1 Å X-ray crystal structure of Omp32 solved by the method of single isomorphous replacement (SIR) and by molecular replacement (MR) of another crystal form. Substantial differences from the structure and electrostatic potential of structurally known porins contribute to and explain the particularly strong anion selectivity of this porin. In addition, we show that Omp32 associates with a peptide to form a stoichiometric complex in the crystallographic asymmetric unit.

Results and discussion

Crystal packing of the porin-peptide complex

Omp32 from *C. acidovorans* crystallized in two crystal forms (CF1 and CF2) both of which are rhombohedral (R3) but showed different unit-cell sizes [26]. CF1 crystals exhibit unit-cell constants $a = b = 107.25$ Å and $c = 140.59$ Å, whereas CF2 crystals have smaller cell constants of $a = b = 87.1$ Å and $c = 135.28$ Å (Tables 1 and 2). The structure of Omp32 was solved by SIR using one K_2PtCl_4 derivative. Two heavy-atom positions were identified and refined using automated difference Patterson analysis

Table 1

X-ray data for Omp32.

Sample	CF1	CF2	K_2PtCl_4
Space group	R3	R3	R3
Unit-cell parameters			
a (Å)	107.25	87.10	107.34
b (Å)	107.25	87.10	107.34
c (Å)	140.60	135.28	140.46
Resolution (Å)	2.1	2.4	3.2
Wavelength (Å)	0.80	0.80	1.541
Completeness			
overall (%)	89.1	96.2	99.8
outermost shell (%)	91.6	94.3	100
R_{merge}			
overall (%)	11.2	8.9	12.5
outermost shell (%)	45.9	37.6	38.1
Water content (%)	73	55	

procedures. A third atom-binding site was found via difference Fourier methods. Following solvent-flattening, this procedure produced an experimental map of sufficient quality to fit the model of OmpF (Protein Data Bank [PDB] accession code 2OMF) and to trace the missing protein portions. The arrangement of protein trimers in both crystal forms is shown in Figure 1a.

CF1 crystals correspond to the type II membrane protein crystals as defined by Michel [29] with large lateral spacings and contacts only between proteins of neighboring crystal layers. The closest lateral distance between two porin trimers is ~23 Å, leaving sufficient space for the formation of toroidal detergent girdles around the nonpolar exterior of the protein. The packing in CF1 closely resembles that of the porins from *Rhodobacter capsulatus* and *Rhodospseudomonas blastica* which both crystallize in the same space group and show similar but small contact areas between neighboring trimers [8,30]. Crystal contacts in the CF1 case are created by weak, hydrophobic monomer-monomer (layer A-layer B) interactions (Figure 1a) that are

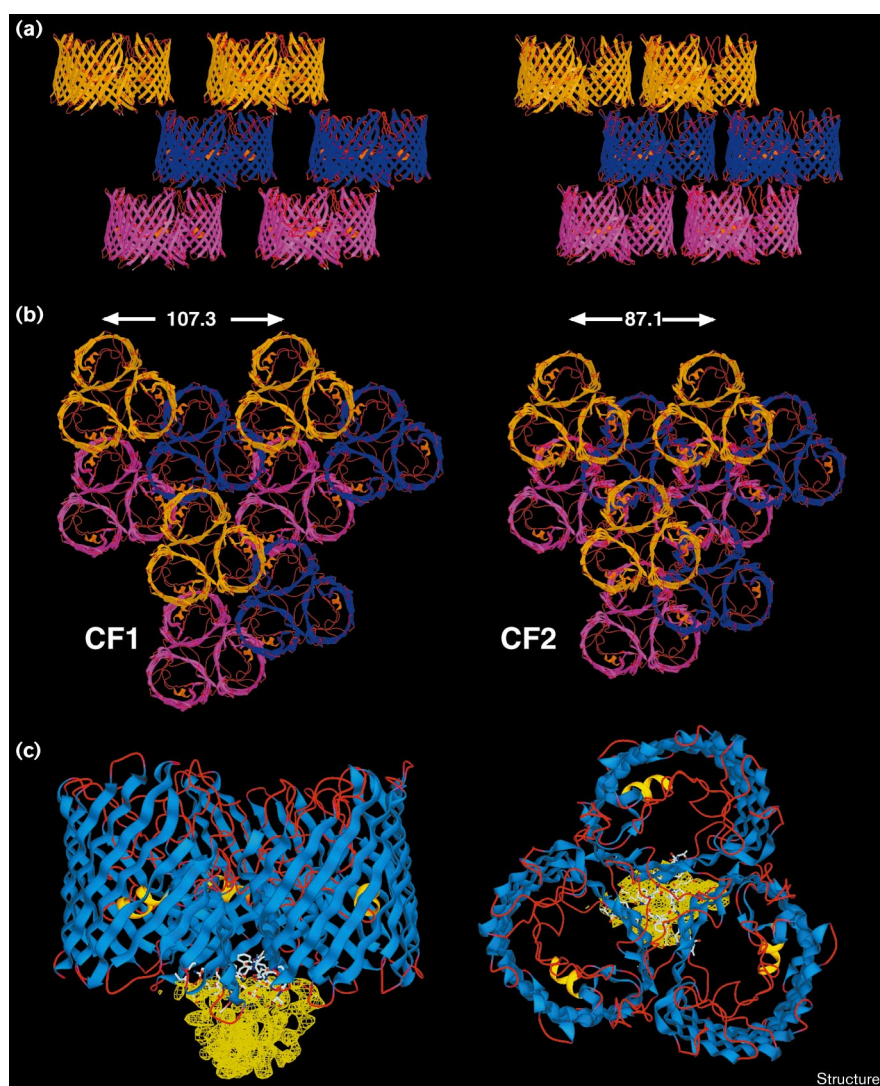
Table 2

Structural data after refinement.

	CF1	CF2
Resolution range (Å)	20–2.1	20–2.4
Unique reflections	31,811	14,928
R factor (R_{free})	0.20 (0.23)	0.24 (0.28)
Number of atoms in refinement		
protein	2480	2480
water	98	34
peptide	60	60
Average B factor of porin (Å ²)	33.6	38.7
Rms deviation from ideality		
bonds (Å)	0.0063	0.0097
angles (°)	1.42	1.78

Figure 1

Porin Omp32 from *C. acidovorans* in crystal forms CF1 and CF2. **(a)** Contact between porin molecules in a view perpendicular to the lattice *z* direction. According to space group R3 there are three laterally shifted and repetitive protein layers of successive *abc-abc* building the protein crystal. Crystal layers are color-coded: orange (*a*), blue (*b*) and magenta (*c*). **(b)** The lateral arrangement of Omp32 trimers. The distance between two points that are related by translational symmetry (marked with double arrows) is 107.3 Å in CF1 and 87.1 Å in CF2 in the *x* and *y* direction. **(c)** The Omp32 trimer displayed in side and top view together with the partly ordered and co-crystallized peptide of 54 amino acids. Only eight residues were modeled (gray stick model) owing to experimentally phased electron density. The remaining, but non-interpretable, portion of electron density is indicated in yellow at a 1σ cutoff calculated to 2.9 Å. Figures were produced using the programs MOLSCRIPT [49] and RASTER3D [50].



mediated by the residues of turn T4 (layer A) and loop L6 (B), and by turn T5 (A) and loop L5 (B).

CF2 crystals correspond to crystals of type I [29] as they contain lateral contacts between adjacent proteins of the same layer. The lateral arrangement reflects the structure of two-dimensional crystals of several membrane proteins including Omp32 [31,32]. The smallest lateral protein-to-protein distance in CF2 crystals is 4.5 Å and may be limited by the repelling forces of several charged lysine residues in the surface loops (see below). In the CF2 crystals many interlayer crystal contacts exist as each monomer projects deeper into the interior of its closest neighbor and also interacts with a second monomer. Corresponding to the larger cell constants, the water content is 73% for CF1 type crystals and only 55% for CF2 type crystals (Tables 1 and 2). Ordered detergent molecules could not be identified,

indicating that Omp32 does not bind β -octylglucoside in a specific manner. Interestingly, other porins showed serendipitous binding sites for detergent molecules [30].

Porin Omp32 usually co-purified with a peptide, forming a porin-peptide complex that was stable during preparation and crystallization. This peptide consists of 54 amino acid residues including an N-terminal pyroglutamate, yielding a mass of 5.8 kDa. The peptide was identified by sodium dodecyl sulfate polyacrylamide gel electrophoresis (SDS-PAGE) of purified Omp32 preparations used for the crystallization (KZ, *et al.*, and HE, unpublished results). Porin (α) plus peptide (β) form an $(\alpha\beta)_3$ homotrimer with an internal C3 symmetry axis, which is identical to the crystallographic axis in both crystal forms (Figure 1b). The asymmetric unit thus contains one $(\alpha\beta)$ complex. Location of the peptide close to the trimer axis

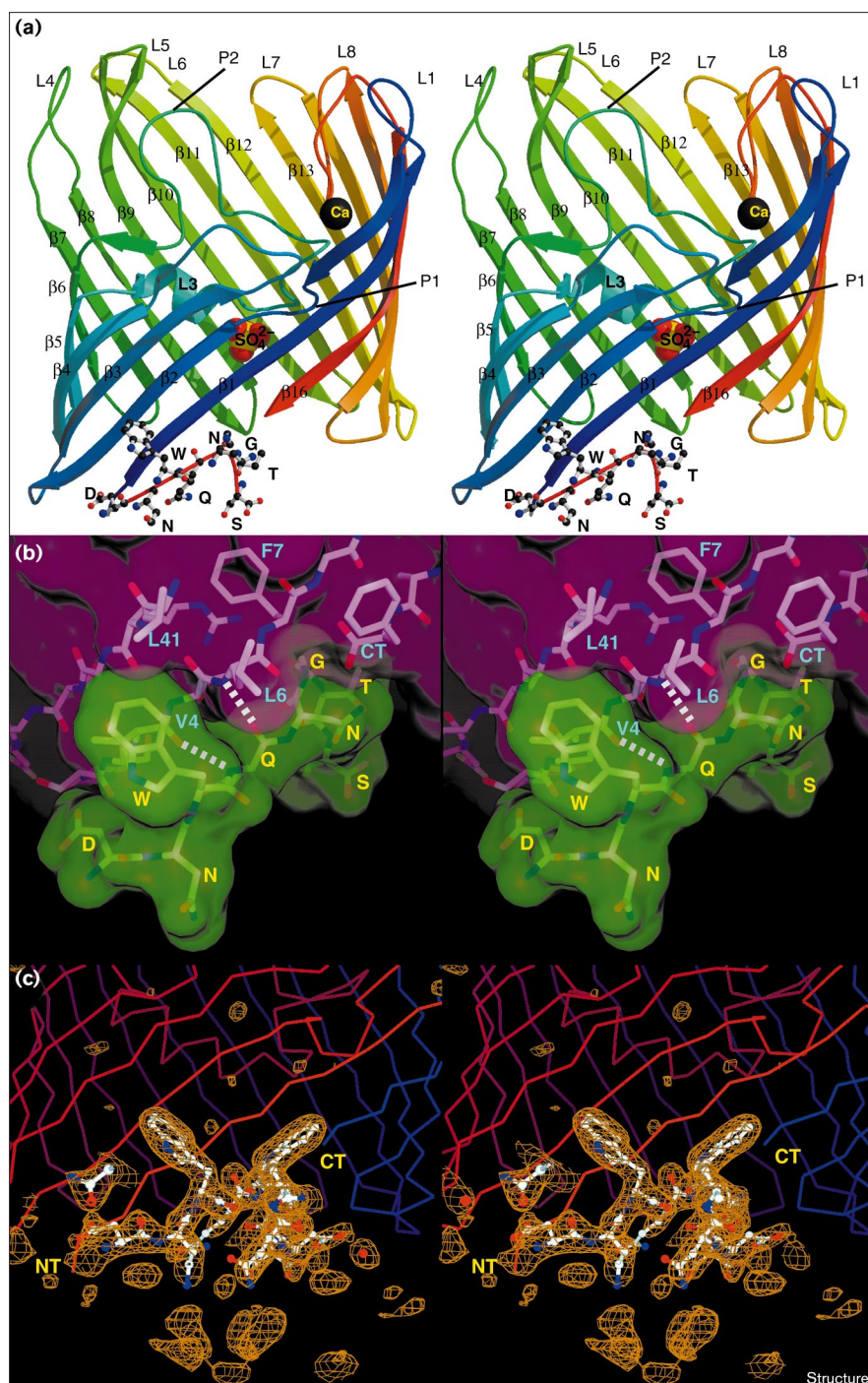
at the periplasmic face of the porin did not disturb crystallization as there is sufficient free space.

Identification of the peptide–protein complex

Eight ordered amino acids could be identified in the $F_o - F_c$ -map of CF1. The peptide sequence Asp-Asn-Trp-Gln-Asn-Gly-Thr-Ser, corresponding to amino acid residues

number 11–18 of the peptide, was modeled into the interpretable electron-density map. This extended peptide segment is closely attached to the C-terminal end of the porin molecule being only 3.5 Å away from the terminal oxygen atom (Figure 2). The peptide is bound via two hydrogen bonds established between CO and NH of the glutamine of the peptide and Leu6 HN and Val4 CO

Figure 2



Overall fold of the monomeric Omp32 together with part of the bound peptide. **(a)** The complex is viewed perpendicular to the trimeric symmetry axis of the porin and illustrates the course of the polypeptide chain and protein–peptide interactions. The colour ramp starts at the N terminus (blue) and ends at the C terminus (red). Strands are labeled with $\beta 1$ – $\beta 16$ and loops with L1–L8. Note that ‘loops’ L5–L7 are actually β turns. The bound Ca^{2+} is marked in black. Eight amino acids (DNWQNGTS; in single-letter amino acid code) of the attached peptide are shown in ball-and-stick representation. The position of the bound SO_4^{2-} within the channel is shown in CPK representation. P1 is a protrusion of six amino acid residues in the middle of β -strand 2 ($\beta 2$) that points towards the channel interior. P2 is a protrusion of L3 towards the external face of the molecule. The model was drawn with MOLSCRIPT [50] and RASTER3D [51]. **(b)** Stereoview close-up showing a surface representation of the contact region between porin (magenta) and the peptide (green). Amino acids involved in the formation of hydrogen bonds (marked as broken lines) are Val4 and Leu6 from Omp32 and glutamine from the peptide. **(c)** Stereoview of the $F_o - F_c$ map calculated at 3.5σ using the porin model phases. The map shows residual electron density. Two of the peptides related by crystallographic symmetry that were modeled using experimental SIRAS and difference model maps are displayed in ball-and-stick representation. The N-terminal (NT) and C-terminal (CT) ends of the porin monomer are marked. The figures in (b,c) were produced with DINO (<http://www.bioz.unibas.ch/~xray/dino>).

from Omp32 (Figure 2b). Moreover, there are interactions between the tryptophan sidechain of the peptide and the hydrophobic cave formed by several porin sidechains close to the porin trimer axis. The tryptophan residue is embedded between the sidechains of Val4, Leu41 and Phe55 of one monomer, and the sidechain of Leu6 of the neighboring monomer. In addition, each peptide molecule forms two hydrogen bonds with each of its crystallographic neighbors in the trimeric complex. The hydrogen-bonding network leads to the formation of a triangular array and contributes to the remarkable stability of the peptide–protein complex.

In Omp32 the N-terminal amino acids are apparently exposed to the periplasm (Figure 2) and not folded back towards the C-terminal phenylalanine as found with OmpF and PhoE from *E. coli* [9]. This free space is occupied by the bound peptide in Omp32, indicating that corresponding porin–peptide interactions cannot be expected for porins of the OmpF type.

Further electron density for the peptide was observed up to 15 Å from the termini of the porin trimer, but this density was not interpretable (Figures 1c,2c). The density apparently does not account for the entire volume of the remaining peptide mass. The complete peptide is homologous to proteobacterial proteins that are involved in linking the outer membrane with the cell wall peptidoglycan but is not related to SLH-domain-containing proteins in particular (KZ, *et al.*, and HE, unpublished results).

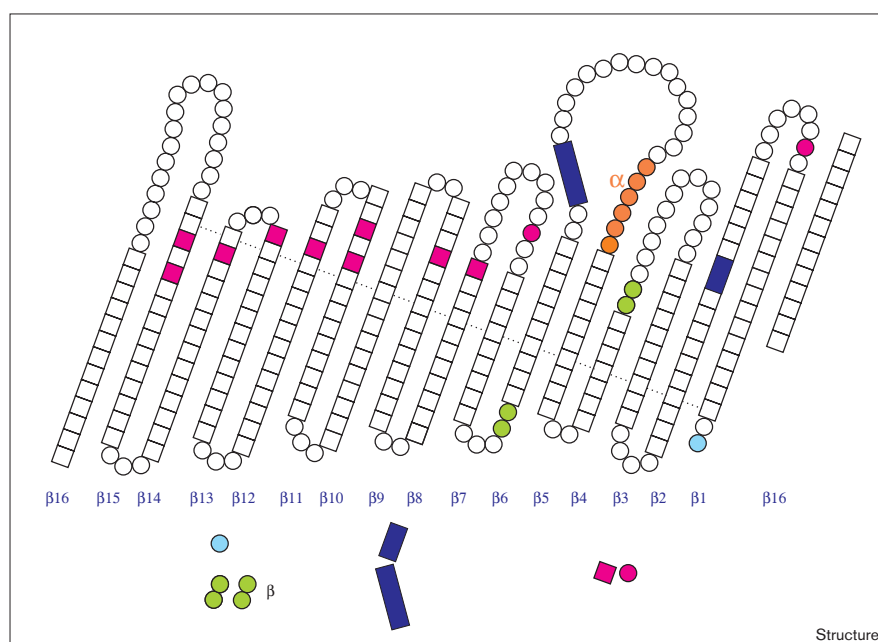
Porin structure description

The final model of Omp32 consists of 332 amino acids including the cyclic pyroglutamate as a nonstandard amino acid at the N terminus [33]. All amino acids of CF1 have mainchain and sidechain density and could be modeled by means of difference and $3F_o - 2F_c$ maps. CF2 crystals showed no density in one loop region nor for many sidechains, and these were not used for the final modeling. The sequence and principle topology of the chain fold is given in Figure 3. The porin monomer is formed by a 16-stranded antiparallel β barrel composed of β strands of between seven (β strand 4; β_4) and 16 (β_2 , β_{10}) residues in length and a tilt of strands between 35° and 52° relative to the trimer axis. Seven short periplasmic turns and eight external loop structures connect the β strands. The shear number of the β barrel is 20 in correspondence to other 16-stranded porins [30].

There are a number of features that are peculiar to this porin. A small protrusion (P1) of six residues in length (32–37) in β_2 is located approximately midway of the barrel height. It protrudes 11 Å from the barrel wall into the pore interior and folds back to continue the β strand (Figures 2,3). The longest loop, L3, contains 44 residues and comprises two structural domains. The first domain folds into the center of the channel along the inner channel wall roughly parallel to the membrane surface, and the second, forming protrusion P2 (residues 118–130), folds towards the rim of the β barrel (Figures 2,3). L3 contains two short, antiparallel β strands at the very beginning and the end of the loop, and a right-handed α helix

Figure 3

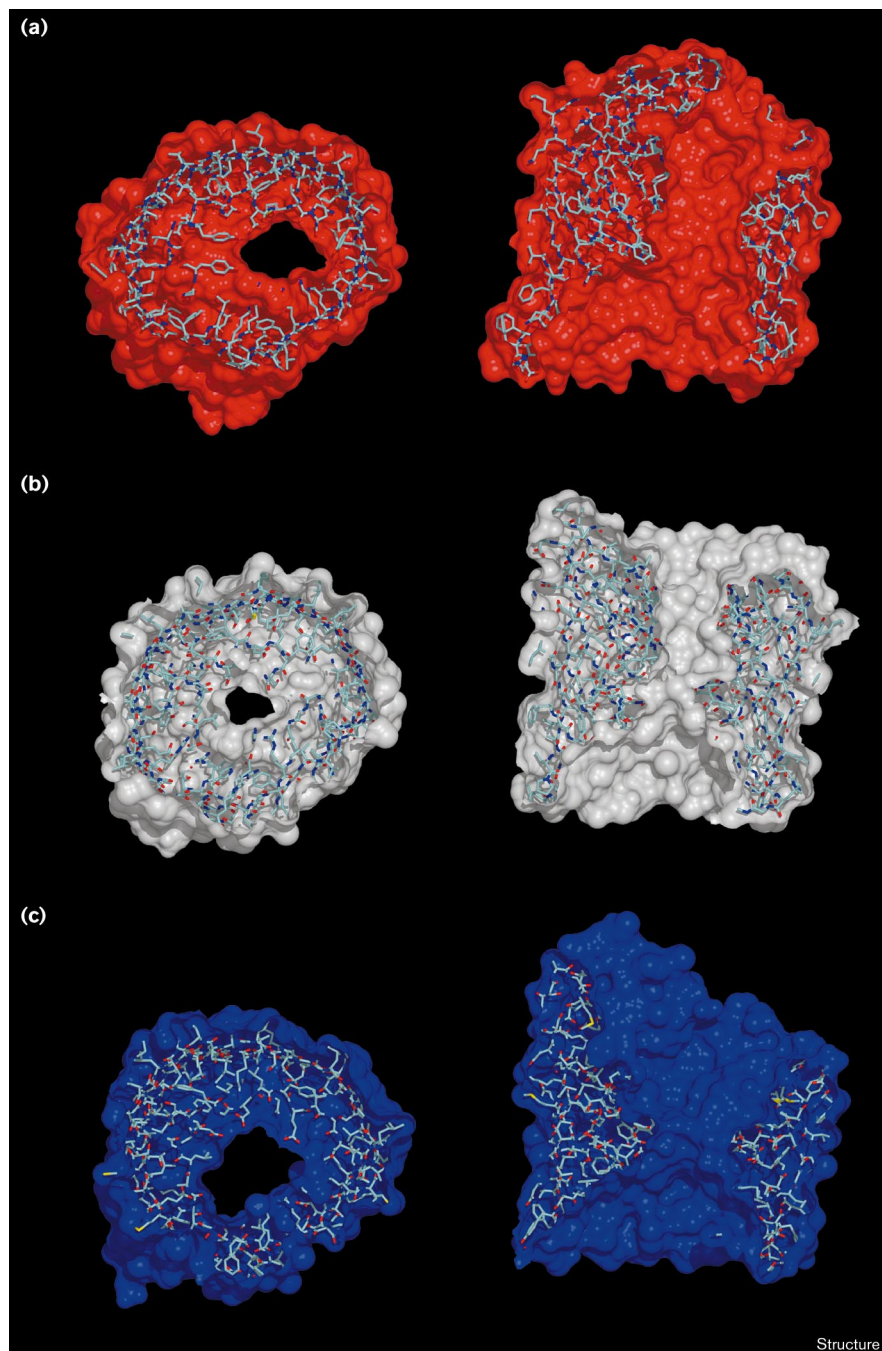
Folding model of the β -barrel structure of Omp32. View from the membrane-exposed side of the 16-stranded β barrel, which is unrolled (β strands β_1 – β_{16}). The C-terminal β strand is repeated to indicate the cyclic structure of the barrel. Amino acids located in β strands are boxed, other structural features are highlighted. L1–L8, external loops; P1 and P2, protrusions; NT, N-terminal amino acid; CT, C-terminal amino acid. Numbers indicate amino acid positions in the sequence.



(residues 96–101) followed by a short 3_{10} helix (residues 102–104). There are several interactions between this portion of L3 and the barrel wall, including three short hydrogen bonds to $\beta 9$ and L5 and a salt bridge between Asp128 and Arg92 of $\beta 5$. The loops L4 and L6, which fold towards the pore in OmpF, do not do so in Omp32; the corresponding space is occupied by protrusion P2. Loop L3 together with the small protrusion P1 determine the dimensions of the constriction site of the channel. The

cross-section of the channel is $5 \times 7 \text{ \AA}$ and, thus, is unusually small compared to values of $7 \times 11 \text{ \AA}$ for OmpF and $10 \times 11 \text{ \AA}$ for the porin of *R. capsulatus* (Figure 4). In fact, no constriction zone of structurally known porins, neither 16-stranded nor 18-stranded ones, is narrower. Loops L5, L6 and L7 are unusually short and essentially consist of β turns with only two or three connecting amino acid residues (Figures 2,3). L8, which is the second longest loop in Omp32 (residues 301–319), folds into the barrel

Figure 4



Porin pore sizes illustrated by central sections. (a) OmpF from *E. coli* (PDB code 2OMF), (b) Omp32 from *C. acidovorans* and (c) the porin from *R. capsulatus* (PDB code 2POR) were superimposed and corresponding sections calculated. Horizontal sections (left panels) through the narrowest site and vertical sections (right panels), showing the progression of the channels, illustrate the channel size inside the molecules and in the constriction zone in particular. Omp32 possesses the narrowest pore cross-section. The structures were superimposed using TOP and the figures were generated using the program DINO (<http://www.bioz.unibas.ch/~xray/dino>).

interior and contributes to the formation of the particularly narrow channel opening at the external side. A hydrogen bond between Lys308 CO and Thr31 NH stabilizes the loop conformation. Moreover, Gly309 CO is one of the five coordinating residues, binding one Ca^{2+} at the monomer–monomer interface. Leu29 CO, the sidechain of Asp64, and the sidechains of Asn136 and Glu158 from the adjacent monomer contribute to the remaining bounds. The position of the Ca^{2+} site corresponds to that found in the *R. capsulatus* porin (PDB code 2POR [8]). The fact that Ca^{2+} is indeed involved in stabilizing the trimeric structure is supported by the observation that EDTA weakens the heat stability of the oligomeric complex [34].

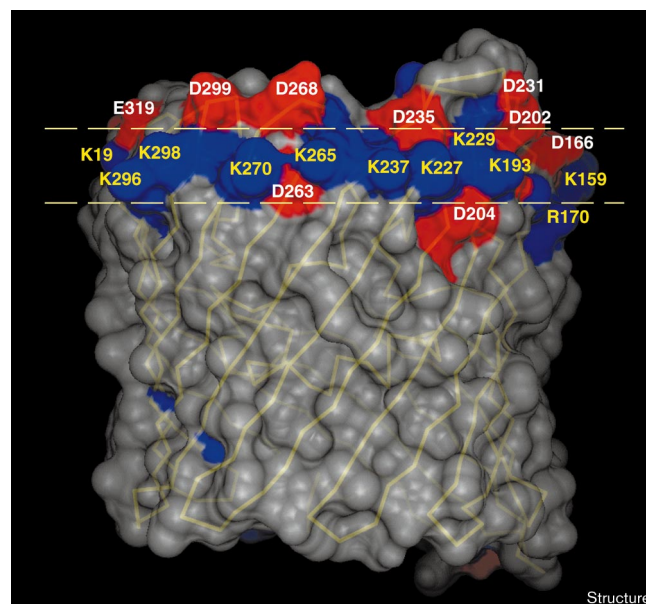
A total of 202 residues (61%) are involved in β -strand formation. The previously assessed amount of $70 \pm 8\%$ using Fourier transform infrared spectroscopy [34] is thus in reasonable agreement with the structural data. Nine residues form two and a half helical turns, and 22 amino acids are located in β turns connecting β strands at the periplasmic side. Omp32 contains 59 charged amino acids (14 arginines, 17 lysines, 20 aspartates and 8 glutamates) plus three histidine residues with an overall positive charge of 4 (including the bound Ca^{2+} and taking into account the missing charge of the N-terminal pyroglutamate). This is a clear difference to the other structurally known porins, which exhibit a surplus of negative charges throughout.

The membrane-exposed surface: aromatic amino acid and lysine girdles

A prominent feature of Omp32, and bacterial outer membrane proteins in general, is the ~ 25 Å high nonpolar belt formed by hydrophobic amino acids, which represents the membrane-exposed part of the barrel. Two girdles of aromatic residues, being less distinct in Omp32, border the belt. The inner or periplasmic ring of aromatic residues consists of three phenylalanine and three tyrosine residues, whereas two phenylalanine and five tyrosine residues define the outer girdle. A characteristic feature of this belt, which is also seen in Omp32, is that phenylalanine residues show a preferential orientation towards the hydrophobic membrane matrix whereas tyrosine residues point towards the polar lipid head group regions. The belt does not surround the entire barrel. Polar as well as apolar residues form the surface that is buried upon trimer formation.

In addition to the nonpolar girdles, we identified a positively charged ring consisting of ten lysine residues (K19, K159, K193, K227, K229, K237, K265, K270, K296 and K298) and one arginine (R170), running 5–8 Å above the outer girdle of aromatic residues (Figure 5). The accumulation of positive charges is at least partly compensated for locally by ten aspartic acid residues (D24, D157, D166, D202, D204, D231, D235, D263, D268 and D299) and one glutamate (E319) that encircle the girdle. *In vivo*, the lysine sidechains and part of the aspartate sidechains point

Figure 5



The surface of Omp32 oriented towards the outer membrane. A girdle of ten lysine residues and one arginine is enveloped by eight visible, oppositely charged aspartate residues and one glutamate residue. The β strands are indicated in yellow. The surface was calculated using the program MSMS [51], and the representation was produced using the program DINO (<http://www.bioz.unibas.ch/~xray/dino>).

towards the hydrophilic and preferably negatively charged lipopolysaccharide (LPS) head groups. The charge ring in conjunction with the aromatic acid residues might serve to impart an increased stability in the vertical positioning of the protein in the outer membrane. The assumption of strong polar porin–LPS interactions is supported by the fact that solubilization of Omp32 by detergents usually failed to remove LPS completely (KZ and HE, unpublished results). In accordance with our observations, the X-ray structure of FhuA in complex with LPS revealed several lysine and arginine residues in proximity of the negatively charged LPS head group [35].

Electrostatic properties of the pore

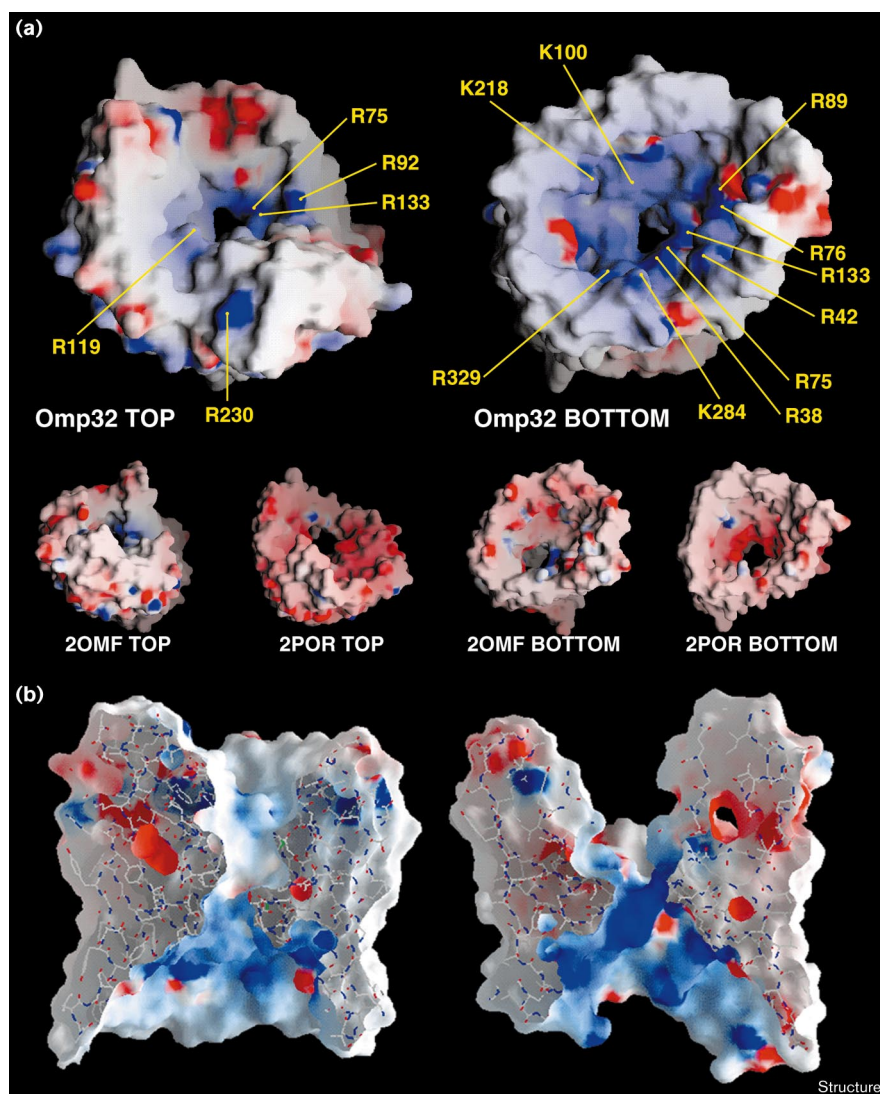
A GRASP representation of the surface potential originating from all charged amino acid residues is shown in Figure 6. At the external side, a number of arginines (R75, R92, R119, R133 and R230) line the pore with their sidechains oriented towards the pore interior. Viewed from the periplasmic side even more amino acid residues contribute to a strong surface potential. Twelve amino acids (R38, R42, K52, R75, R76, R89, K100, R133, K218, K256, K284 and R329) create a positively charged surface with little compensatory effect provided by a few negative countercharges. A ladder of five positively charged residues (K74, R92, R133, R75 and R38) extends from the external to the periplasmic side of the channel, passing through the

constriction zone and creating a strong positive potential inside the narrow channel (Figure 6). Because of the lack of acidic residues within the constriction zone there cannot be a strong transverse electric field in the channel (Figure 6b); the existence of such a field was first predicted in the *R. capsulatus* porin on the basis of electrostatic calculations [9]. As a consequence, the positive potential is not attenuated in Omp32 and therefore represents a strong attractor for anions and repels cations, whereas the electrostatic field in the *R. capsulatus* porin apparently facilitates the diffusion of molecules possessing a dipole moment [30]. Difference maps showed a significant spherical electron density located in the constriction zone, which could be modeled as sulfate ion (Figure 7). Sulfate salts were highly concentrated constituents of the crystallization buffer. The anion is apparently bound via two hydrogen bonds to Arg38 Ne with S–O distances of 2.95 Å;

Arg38 (next to Arg75) is located at the narrowest part of the constriction zone. It is conceivable that organic anions of greater physiological significance are bound here *in vivo*.

Arginine residues in the vicinity of the pore constriction zone are conserved in bacterial porins in general, and within the β -subdivision in particular (see below). Comparing all structurally known porins, however, only Omp32 possesses a clear majority of positive charges inside the channel, at the external and the periplasmic pore entrance. As shown in Figure 6a, other porins exhibit a negative surface potential in accordance with a surplus of negatively charged amino acids and a functional cation selectivity [2]. This illustrates that the property of ion-selectivity among porins is not primarily determined by the presence or absence of positive charges, but rather by the variable content of aspartate

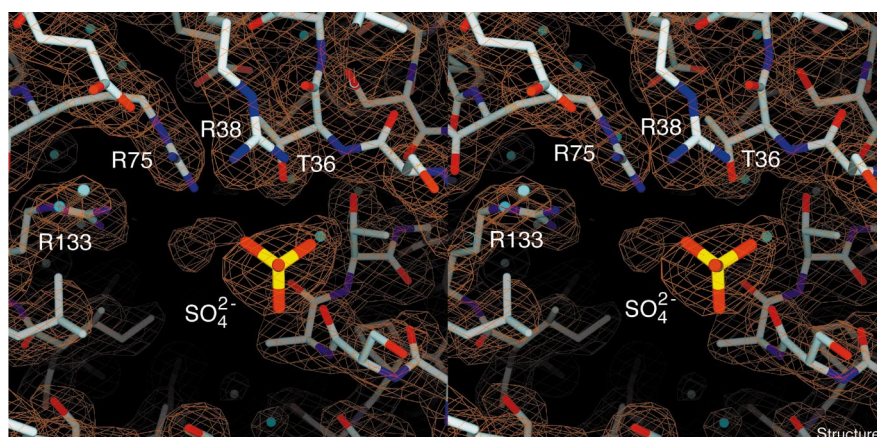
Figure 6



GRASP molecular surface representations of Omp32. **(a)** The porin is shown from the top (external face) and bottom (periplasmic face) of the molecule. The molecular surface is colored according to electrostatic potential: blue, positive; red, negative; and white, uncharged. The positions of positively charged residues that make a significant contribution to the surface potential are indicated. For comparison, the electrostatic surface potentials of OmpF (2OMF) and the *R. capsulatus* porin (2POR) are displayed. **(b)** Longitudinal sections along the middle of the Omp32 channel. Left side: View onto the back side of the channel (wall facing the membrane). Right side: view onto the inner side of the channel (wall facing the symmetry axis in the trimeric complex). Note the particularly strong positive potential in the constriction site, representing the charge filter created by residues Arg133, Arg75 and Arg38. The figures were generated using the program GRASP [52].

Figure 7

Sulfate-binding site inside the channel of Omp32. Stereo plot of the final electron density of sulfate, water molecules and the surrounding protein. The $2F_o - F_c$ map is contoured at 1.0σ and calculated at 2.1 \AA . The channel section is shown from the periplasmic side of the constriction zone. Protein and sulfate are displayed in ball-and-stick representation (color-coded by atom type). Three conserved arginine residues (Arg38, Arg75 and Arg133) are indicated. The sulfate ion is bound to Arg38. Thr36 located in the small protrusion P1 is marked to illustrate its contribution to channel constriction.



and glutamate residues that either compensate or over-compensate the conserved arginines.

Structure–function relationships

The accumulation of positive charges inside the channel is consistent with the strong anion selectivity of Omp32 observed in conductance measurements with the porin reconstituted into planar lipid membranes [25]. The apparent ratio of permeability coefficients for anions to cations P_{Cl^-}/P_{K^+} is about 17, as determined when a gradient of 9–3 mM KCl was applied to a membrane containing Omp32. Approximately 94% of the diffusing ions are Cl^- under these conditions. Chemical modification of arginine residues and the studies of the pH-dependent selectivity of the closely related porin Omp34 from *Acidovorax delafieldii* suggested that the positive charges of arginines represent the major selectivity filter inside the channel, whereas lysines contributed only marginally [16]. The situation with Omp32 and Omp34 is in contrast to the moderately anion-selective porin PhoE from *E. coli*, where a number of arginine residues are inside the channel but a single lysine contributes most to the selectivity [9,36]. Although the charges of Arg38, Arg75 and Arg133 make up the core of the anion filter within the constriction zone of Omp32, the particularly small cross-section of the channel enhances the selectivity further. In addition, Leu94 and Ile132 are situated opposite to the hydrophilic region in the constriction zone and force ions to pass the charge filter even more closely; this arrangement might facilitate the diffusion of organic anions with moderately amphiphilic character.

The accumulation of protein charges inside the channel and the resulting electrostatic field have consequences for the penetration of ions, particularly at low salt concentrations when ions do not shield protein charges effectively. This was shown for KCl concentrations below 100 mM with increasing effects down to 3 mM [25]. Voltage-current

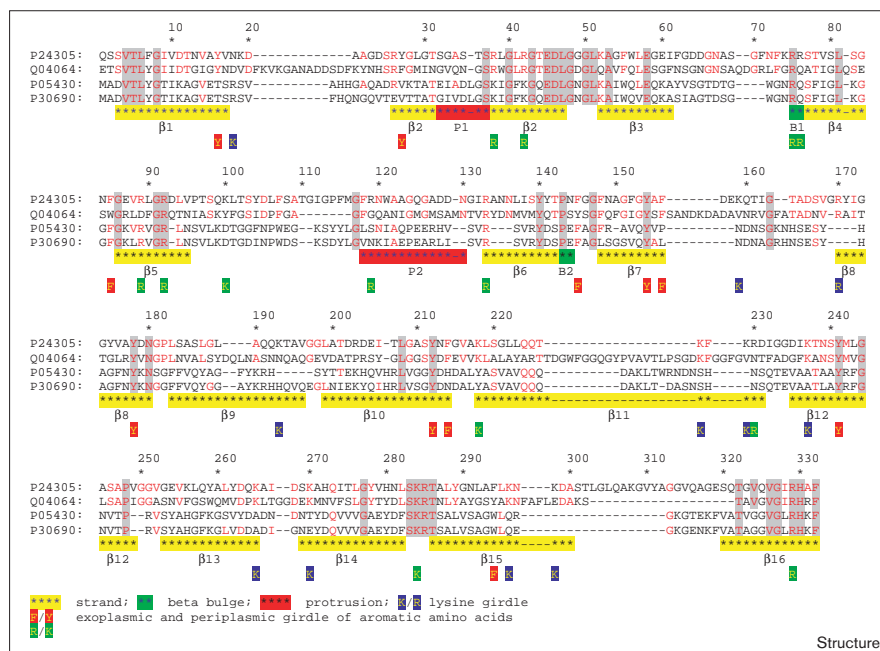
curves are nonlinear in low salt (independent of and different to the phenomenon of voltage-dependent channel closing) resulting in variable voltage-dependent conductance characteristics. This behavior, also being valid for porin Omp34 from *A. delafieldii* [37], can be attributed to effects of the electrostatic potential. Salt concentration dependent effects were also recently reported for OmpK36, the cation selective porin from *Klebsiella pneumoniae*, where shielding of protein charges in high salt concentrations affects the strength of ion selectivity [12,38].

Porin Omp32, as well as Omp34, excludes larger organic molecules like oligosaccharides [39] but appears large enough to accommodate organic acids, as judged from their molecular dimensions. Similar to the situation with sugar-specific porins, which exhibit smaller cross-sections than OmpF [6], elongated molecules (e.g., oligosaccharides in the case of maltoporin) may pass the constriction zone if they are aligned with the longitudinal pore axis [5,6]. It is thus tempting to speculate that the apparent longitudinal electrostatic field in the pore of Omp32, which is created by the gradient of positive charges from the exoplasmic to the periplasmic face, and the ladder of arginines along the pore constriction contribute to a favorable orientation of organic anions inside the channel.

Homologous porins

Omp32 shows sequence identity and similarity to several bacterial porins, as illustrated in Figure 8, and even to the eukaryotic voltage-dependent anion channels (~60% similarity; results not shown). Particularly high sequence similarity is seen with porins of pathogenic species from *Bordetella* and *Neisseria*, which are also members of the β -subdivision of proteobacteria. The greatest similarity is to the porin from *B. pertussis* which shares 38% identity and 70% similarity. Homology appears more distant to the porins of *N. meningitidis* (24% identity; 64% similarity) and *N. gonorrhoeae* (25%; 60%).

Figure 8



Amino acid sequence alignment of homologous porins selected from the β -subdivision of proteobacteria. Omp32 from *C. acidovorans* (GenBank accession code P24305), the outer membrane protein of *B. pertussis* (Q04064), the major outer membrane protein PI.A from *N. gonorrhoeae* (P05430) and major outer membrane protein PI.B from *N. meningitidis* (P30690) are compared. The numbers refer to the sequence of Omp32. Highly conserved residues are highlighted in red type. Secondary structure elements are indicated: β strands are indicated by yellow bars, β bulges B1 and B2 are marked with green bars and the protrusions P1 and P2 are marked in red. Amino acids that contribute to the positive surface potential within the pore and the two girdles of aromatic amino acids are marked as described in the figure. Pairwise sequence alignments were generated using ToPLign (<http://cartan.gmd.de/ToPLign.html>).

Large variations in sequence are detected in the external loops but only small variations are seen in turn regions, an observation already made for other porins and the eight-stranded β -barrel proteins that form the β 8 family of outer membrane proteins [40]. Turn 1 and turn 7 (T1 and T7) situated in the trimer contact region are more conserved than the others. Interestingly, residues 45–53 and 283–286 of Omp32 (which contain T1 and T7) contribute to a network of polar and nonpolar interactions between the interfaces of adjacent monomers. These clusters of amino acids are almost invariable (Figure 8) and might therefore have an essential role in monomer–monomer contact formation in porins of β -proteobacteria. Regarding the fully conserved residues, we find aromatic residues in the girdles (Figure 8), a number of glycines preferentially in turns, and two conserved proline residues in β strands. Most of the arginine residues located in the pore interior, and in particular those forming the arginine ladder in Omp32 (Arg38, Arg75 and Arg133), are strictly conserved. These residues were observed in many other porins including the cation selective OmpF from *E. coli* and OmpK36 from *K. pneumoniae*, with a few Arg→Lys exchanges. Arg133 and Arg38 of Omp32 could be aligned Arg132 and Arg42 of OmpF by sequence and structure comparisons. Arg75 of Omp32 shows positional and structural homology to Arg82 in OmpF but was less reliably aligned by sequence alignments. Arg92 marks the position where L3 folds into the β barrel and forms a structurally conserved salt bridge to Asp128; in OmpF the corresponding residues are Arg100 and Asp126. It is an interesting observation that the structures and sequences of Omp32

and OmpF do not align very well (data not shown). For example, Trp56 of Omp32 is exposed to the channel lumen, but aligns with Trp61 of OmpF which faces the trimer contact region.

The amino acids Val4 and Leu6 of β -strand 1, which closely interact with the tryptophan residues of the bound peptides, are invariable in porins of β -proteobacteria but not in the porins of organisms from other subdivisions. In turn, the tryptophan residue of the peptide is conserved in homologous proteins (KZ, *et al.*, and HE, unpublished results).

The structural similarity of Omp32 is greatest to OmpF (PDB code 2OMF) as judged by the superimposition of C α atoms. A total of 214 C α positions, which contain almost all of the 207 β -strand amino acids, were structurally aligned in the fit and gave an average root mean square (rms) deviation of 1.35 Å. Using the coordinates of the *R. capsulatus* porin (PDB code 2POR) 189 C α positions could be aligned with an rms value of 1.72 Å, reflecting a stronger structural deviation. In retrospect, the failure of MR calculations, using the coordinates of OmpF as a model, must be attributed to the fairly high rms deviation of even those parts in best agreement in the β -barrel region.

Biological implications

Bacterial porins provide pores in the outer membrane of Gram-negative bacteria and in some cases exhibit strong selectivity or even specificity for molecules. In porin Omp32 from *Comamonas (Delftia) acidovorans* the combination of a particularly narrow constriction zone,

together with the placement of several arginine residues inside the pore, creates a strong positive potential and provides an effective charge filter that appears even to have the capability to bind divalent anions. Porins like Omp32 would facilitate the selective influx of anions into the periplasm, if equally sized ions of opposite charges were present in the surrounding medium and the translocated ions were continuously removed from the periplasm (e.g. by specific transport into the cell). The accumulation of inorganic anions such as Cl⁻, however, is not a physiological requirement for *C. acidovorans*.

The strong anion selectivity of Omp32, which can be deduced from the structure and which is found in conductivity measurements, rather suggests the functional selection of slowly diffusing (i.e. larger anions), which are taken up together with smaller cations at similar rates for reasons of electroneutrality. Omp32, the major and constitutively expressed porin of *C. acidovorans*, shows structural features that illustrate the adaptation to negatively charged ions such as organic acids — the preferred carbon source of this acid-consuming organism and related species [27].

Omp32 specifically binds a peptide at its periplasmic face close to the symmetry axis of the homotrimer. This is the first direct proof that porins bind periplasmic proteins, presumably being involved in coupling the outer membrane to the peptidoglycan of the cell wall. In this respect Omp32 represents a link between porins such as OmpF from *E. coli* that do not bind periplasmic peptides and those possessing a periplasmic domain with peptidoglycan-binding activity, such as cyanoporins and the *Thermus thermophilus* porin. The trimeric structure of porins is clearly of advantage in stabilizing porin-peptide interactions.

Materials and methods

Purification and crystallization of porin Omp32

Porin Omp32 was solubilized using isolated outer membranes from the bacterium *C. acidovorans* (Deutsche Sammlung von Mikroorganismen und Zellen, DSMZ, No. 39). Omp32 was solubilized with octyl-polyoxyethylene (OPOE) and purified by gel-filtration and anion-exchange chromatography as described previously [26]. The porin was dialyzed against crystallization buffer, containing 2% β-D-octylglucoside to exchange the detergent, and crystallized as described in detail by Zeth et al. [26].

X-ray analysis, structure determination and refinement

Crystallization yielded two crystal forms CF1 and CF2 that were used for structure analysis [26]. All X-ray data presented were collected at room temperature. Native data sets of both crystal forms were collected at DESY (Deutsches Elektronen-Synchrotron) beamlines BW6 and X31 using a MAR345 image-plate detector system (MAR research system). X-ray data of the derivative using type CF1 crystals were collected on an area detector (STOE, Darmstadt) at a rotating anode (Schneider, Offenburg) with CuK_α radiation. Diffraction data were processed using the programs XDS [41] and DENZO [42]. Collection of phasing information via the MR method using the rotation function of the program package X-PLOR [43] and the porin models available at that time (PDB entries 2OMF, 2POR and 1PRN) failed. In order to obtain initial phasing information, protein crystals of form CF1 were soaked with 5 mM K₂PtCl₄ for

24 h. One major and two minor heavy-atom binding sites were identified via difference Patterson techniques and refined using the programs Darefi [44] and SOLVE [45]. The best phase determination and heavy-atom refinement was obtained by SHARP [46] followed by solvent-flattening using the package SOLOMON from the CCP4 package [47]. The overall figure of merit (FOM) was 0.51–3 Å.

An amino acid sequence alignment of Omp32 and OmpF predicted 20% sequence identity and 65% similarity. The OmpF model was therefore placed into the initial solvent-flattened electron density. Being aware of building a model with a strong model bias, experimental phases were used for initial cycles of model rebuilding and refinement. As soon as the R_f dropped to below 30% $2F_o - F_c$ and $F_o - F_c$ maps were further used for improvement of the model.

Model rebuilding and refinement using X-PLOR and CNS [48] was performed over several cycles. Electron density of type CF1 crystals showed the backbone and all of the sidechain signals. In contrast, the type CF2 structure lacked clear mainchain and sidechain density in several places.

An initially unexplained electron density observed in $3F_o - 2F_c$ and $F_o - F_c$ maps was carefully analyzed and a small peptide of eight amino acids was identified and inserted into the structure. The peptide was isolated and sequenced as described elsewhere (KZ, et al., and HE, unpublished results), and its size was confirmed by electron-spray ionization (ESI) mass spectroscopy.

Finally, water molecules were identified in the refined structure and inserted into peak densities of 3.5σ located in $F_o - F_c$ maps, using an automatic CNS procedure. The structure of type CF2 crystals was solved by MR using the cross-rotation function of the structure of type CF1 crystals refined by application of the CNS package. The final R factor for the model from CF1-type crystals was 20.0% (R_{free} 23.2%) and from CF2-type crystals was 24.0% (R_{free} 28%).

Sequence alignment

Sequence alignments of Omp32 with other porin sequences were performed using FASTA3 and ToPLign (<http://cartan.gmd.de/ToPLign.html>) for pairwise alignments of selected porin sequences from *Neisseria* and *Bordetella* species.

Accession numbers

The coordinates and structure factors for Omp32 have been deposited with the Protein Data Bank (accession code IE54).

Acknowledgements

We thank Wolfgang Baumeister for continuous support. The project was supported by grants of the Deutsche Forschungsgemeinschaft SFB266/D4 and DFG En144/2-1.

References

- Schirmer, T. (1998). General and specific porins from bacterial outer membranes. *J. Struct. Biol.* **121**, 101-109.
- Jap, B.K. & Walian, P.J. (1996). Structure and functional mechanisms of porins. *Physiol. Rev.* **76**, 1073-1088.
- Benz, R. (1994). Permeation of hydrophilic solutes through mitochondrial outer membranes: review on mitochondrial porins. *Biochim. Biophys. Acta* **551**, 238-247.
- Nikaido, H. (1994). Porins and specific diffusion channels in bacterial outer membranes. *J. Biol. Chem.* **269**, 3905-3908.
- Forst, D., Welte, W., Wacker, T. & Diederichs, K. (1998). Structure of the sucrose-specific porin ScrY from *Salmonella typhimurium* and its complex with sucrose. *Nat. Struct. Biol.* **5**, 37-46.
- Schirmer, T., Keller, T.A., Wang, Y.-F. & Rosenbusch, J.P. (1995). Structural basis for sugar translocation through maltoporin channels at 3.1 Å resolution. *Science* **267**, 512-514.
- Pajatsch, M., Andersen, C., Mathes, A., Böck, A., Benz, R. & Engelhardt, H. (1999). Properties of a cyclodextrin-specific, unusual porin from *Klebsiella oxytoca*. *J. Biol. Chem.* **265**, 25159-25166.

8. Weiss, M., Abele, U., Weckesser, J., Welte, W., Schiltz, E. & Schulz, G.E. (1991). Molecular architecture and electrostatic properties of a bacterial porin. *Science* **254**, 1627-1630.
9. Cowan, S.E., et al., & Rosenbusch, J.P. (1992). Crystal structures explain functional properties of two *E. coli* porins. *Nature* **358**, 727-733.
10. Kreusch, A. & Schulz, G.E. (1994). Refined structure of the porin from *Rhodopseudomonas blastica*. Comparison with the porin from *Rhodobacter capsulatus*. *J. Mol. Biol.* **243**, 891-905.
11. Hirsch, A., et al., & Welte, W. (1997). The structure of porin from *Paracoccus denitrificans* at 3.1 Å resolution. *FEBS Lett.* **404**, 208-210.
12. Dutzler, R., et al., & Schirmer, T. (1999). Crystal structure and functional characterisation of OmpK36, the osmoporin of *Klebsiella pneumoniae*. *Structure* **7**, 425-434.
13. Lou, K.-L., et al., & Schirmer, T. (1996). Structural and functional characterisation of OmpF porin mutants selected for larger pore size. I. Crystallographic analysis. *J. Biol. Chem.* **271**, 20669-20675.
14. Saint, N., Lou, K.-L., Widmer, C., Luckey, M., Schirmer, T. & Rosenbusch, J.P. (1996). Structural and functional characterisation of OmpF porin mutants selected for larger pore size. II. Functional characterization. *J. Biol. Chem.* **271**, 20676-20680.
15. Watanabe, M., Rosenbusch, J., Schirmer, T. & Karplus, M. (1997). Computer simulation of the OmpF porin from the outer membrane of *Escherichia coli*. *Biophys. J.* **72**, 2094-2102.
16. Brunen, M. & Engelhardt, H. (1995). Significance of positively charged amino acids for the function of the *Acidovorax delafieldii* porin Omp34. *FEMS Microbiol. Lett.* **126**, 127-132.
17. Brunen, M. & Engelhardt, H. (1993). Asymmetry of orientation and voltage gating of the *Acidovorax delafieldii* porin Omp34 in lipid bilayers. *Eur. J. Biochem.* **212**, 29-135.
18. Bainbridge, G., Mobasher, M., Armstrong, G.A., Lea, E.J.A. & Lakey, J.H. (1998). Voltage-gating of *Escherichia coli* porin: a cysteine-scanning mutagenesis study of loop 3. *J. Mol. Biol.* **275**, 171-176.
19. Mathes, A. & Engelhardt, H. (1998). Voltage-dependent closing of porin channels: analysis of relaxation kinetics. *J. Membrane Biol.* **165**, 11-18.
20. Neumann, U., Benz, R., Rosenbusch, J.P., Stahl, B. & Weckesser, J. (1995). Porin and porin-associated protein (PAP) of *Rhodospirillum rubrum* FR1. *Microbiology* **141**, 3155-3160.
21. Braun, V. & Wu, H.C. (1994). Lipoproteins, structure, function, biosynthesis and model for protein export. In *Bacterial Cell Wall*. (J.-M. Ghuyssen & R. Hakenbeck, eds.). New Comprehensive Biochemistry Vol. 27, pp. 319-341. Elsevier, Amsterdam, The Netherlands.
22. Koebnik, R. (1995). Proposal for a peptidoglycan-associating α -helical motif in the C-terminal regions of some bacterial cell-surface proteins. *Mol. Microbiol.* **16**, 1269-1270.
23. Lupas, A., Engelhardt, H., Peters, J., Santarius, U., Volker, S. & Baumeister, W. (1994). Domain structure of the *Acetogenium kivui* surface layer revealed by electron microscopy and sequence analysis. *J. Bacteriol.* **176**, 1224-1233.
24. Engelhardt, H. & Peters, J. (1998). Structural research on surface layers – a focus on stability, surface layer homology domains, and surface layer-cell wall interactions. *J. Struct. Biol.* **124**, 276-302.
25. Mathes, A. & Engelhardt, H. (1998). Nonlinear and asymmetric open channel characteristics of an ion-selective porin in planar lipid membranes. *Biophys. J.* **75**, 1255-1262.
26. Zeth, K., Schnaible, V., Przybylski, M., Welte, W., Diederichs, K. & Engelhardt, H. (1998). Crystallization and preliminary X-ray crystallographic studies of the native and chemically modified anion-selective porin from *Comamonas acidovorans*. *Acta Crystallogr. D* **54**, 650-653.
27. Wen, A.M., Fegan, M., Hayward, C., Chakraborty, S. & Sly, L. (1999). Phylogenetic relationships among members of the *Comamonadaceae*, and description of *Delftia acidovorans* (den Dooren de Jong 1926 and Tamaoka et al., 1987) gen. nov., comb. nov. *Int. J. Syst. Bacteriol.* **49**, 557-576.
28. Müller, A., Günther, D., Dux, F., Naumann, M., Meyer, T.F. & Rudel, T. (1999). Neisserial porin (PorB) causes rapid calcium influx in target cells and induces apoptosis by activation of cysteine proteases. *EMBO J.* **18**, 339-352.
29. Michel, H. (1983). Crystallization of membrane proteins. *Trends Biochem. Sci.* **8**, 56-59.
30. Kreusch, A., Neubüser, A., Schiltz, E., Weckesser, J. & Schulz, G.E. (1994). Structure of the membrane channel porin from *Rhodopseudomonas blastica* at 2.0 Å resolution. *Protein Sci.* **3**, 58-63.
31. Jap, B.K., et al., & Engel, A. (1992). 2D crystallization: from art to science. *Ultramicroscopy* **46**, 45-84.
32. Engelhardt, H., Scheybani, T., von Gustedt, W. & Baumeister, W. (1994). Formation of two-dimensional crystals of membrane-anchored and water-soluble proteins. In *Biomolecular Materials by Design*. (Bayley, H., Kaplan, D. & Navia, M., eds), Vol. 330, pp. 201-208, Materials Research Society, Pittsburgh, USA.
33. Gerbl-Rieger, S., Peters, J., Kellermann, J., Lottspeich, F. & Baumeister, W. (1991). Nucleotide and derived amino acid sequences of the major porin of *Comamonas acidovorans* and comparison of porin primary structures. *J. Bacteriol.* **173**, 2196-2205.
34. Engelhardt, H., Gerbl-Rieger, S., Krezmar, D., Scheider-Voss, S., Engel, A. & Baumeister, W. (1990). Structural properties of the outer membrane and the regular surface protein of *Comamonas acidovorans*. *J. Struct. Biol.* **105**, 92-102.
35. Ferguson, A.D., Hofmann, E., Coulton, J.W., Diederichs, K. & Welte, W. (1998). Siderophore-mediated iron transport: crystal structure of FhuA with bound lipopolysaccharide. *Science* **282**, 2215-2220.
36. Bauer, K., Struyvé, M., Bosch, D., Benz, R. & Tommassen, J. (1989). One single lysine residue is responsible for the special interaction between polyphosphate and the outer membrane porin PheE of *Escherichia coli*. *J. Biol. Chem.* **264**, 16393-16398.
37. Brunen, M., Engelhardt, H., Schmid, A. & Benz, R. (1991). The major outer membrane protein of *Acidovorax delafieldii* is an anion-selective porin. *J. Bacteriol.* **173**, 4182-4187.
38. Schirmer, T. & Phale, P.S. (1999). Brownian dynamics simulation of ion flow through porin channels. *J. Mol. Biol.* **294**, 1159-1167.
39. Brunen, M. (1992). *Das porenbildende Protein Omp34 von Acidovorax delafieldii: Struktur und Funktion eines typischen bakteriellen Porins und ihre Bedeutung für die lebende Zelle*. PhD Thesis, Technical University of Munich, Germany.
40. Baldermann, C., Lupas, A., Lubieniecki, J. & Engelhardt, H. (1998). The regulated outer membrane protein Omp21 from *Comamonas acidovorans* is identified as a member of a new family of eight-stranded β -sheet proteins by its sequence and properties. *J. Bacteriol.* **180**, 3741-3749.
41. Kabsch, W.J. (1988). Evaluation of single crystal X-ray diffraction data from a position sensitive detector. *Appl. Crystallogr.* **21**, 916-924.
42. Otwinowski, Z. & Minor, W. (1993). *DENZO: A Film Processing Program For Macromolecular Crystallography*. Yale University Press, New Haven, CT.
43. Brünger, A.T. (1992). *X-PLOR 3.1*. Yale University Press, New Haven, CT.
44. Diederichs, K.A. (1994). A comparison of some heavy-atom refinement and phasing programs. *CCP4/ESF-EACBM Newsletters on Protein Crystallography* **31**, 23-30.
45. Terwilliger, T.C. & Berendzen, J. (1999). Automated structure solution of MIR and MAD. *Acta Crystallogr. D* **55**, 849-861.
46. de La Fortelle, E. & Bricogne, G. (1997). Maximum-likelihood heavy-atom parameter refinement in the MIR and MAD methods. *Methods Enzymol.* **276**, 472-494.
47. Bailey, S. (1994). The CCP4 suite of programs for protein crystallography. *Acta Crystallogr. D* **50**, 760-763.
48. Brünger, A.T., et al., & Warren, G.L. (1998). Crystallography and NMR systems: a new software suite for macromolecular structure determination. *Acta Crystallogr. D* **54**, 905-921.
49. Kraulis, P.J. (1991). MOLSCRIPT: a program to produce both detailed and schematic plots of protein structures. *J. Appl. Crystallogr.* **24**, 946-950.
50. Merrit, E.A. & Murphy, M.E.P. (1994). RASTER3D version 2.0: a program for photorealistic molecular graphics. *Acta Crystallogr. D* **50**, 869-873.
51. Sanner, M.F., Olson, A.J. & Spehner, J.C. (1996). Reduced surface: an efficient way to compute molecular surfaces. *Biopolymers* **38**, 305-320.
52. Nicholls, A., Sharp, K.A. & Honig, B. (1991). Protein folding and association: insights from the interfacial and thermodynamic properties of hydrocarbons. *Proteins* **11**, 281-296.

Because Structure with Folding & Design operates a 'Continuous Publication System' for Research Papers, this paper has been published on the internet before being printed (accessed from <http://biomednet.com/cbiology/str>). For further information, see the explanation on the contents page.